Surface Atom Motion to Move Iron Nanocrystals through Constrictions in Carbon Nanotubes under the Action of an Electric Current

Sinisa Coh,* Will Gannett, A. Zettl, Marvin L. Cohen, and Steven G. Louie

Department of Physics, University of California at Berkeley and Materials Sciences Division, Lawrence Berkeley National Laboratory, Berkeley, California 94720, USA

(Received 21 February 2013; published 29 April 2013)

Under the application of electrical currents, metal nanocrystals inside carbon nanotubes can be bodily transported. We examine experimentally and theoretically how an iron nanocrystal can pass through a constriction in the carbon nanotube with a smaller cross-sectional area than the nanocrystal itself. Remarkably, through *in situ* transmission electron imaging and diffraction, we find that, while passing through a constriction, the nanocrystal remains largely solid and crystalline and the carbon nanotube is unaffected. We account for this behavior by a pattern of iron atom motion and rearrangement on the surface of the nanocrystal. The nanocrystal motion can be described with a model whose parameters are nearly independent of the nanocrystal length, area, temperature, and electromigration force magnitude. We predict that metal nanocrystals can move through complex geometries and constrictions, with implications for both nanomechanics and tunable synthesis of metal nanoparticles.

DOI: 10.1103/PhysRevLett.110.185901 PACS numbers: 66.30.Qa, 61.48.De, 66.30.Pa, 73.63.Fg

Electric current induced movement of metal nanocrystals in and on multiwall carbon nanotubes has been observed for many metals, including iron [1–4], copper [5], tungsten [6], indium [7], and gallium [8]. The direction of movement is directly related to the direction of the applied current and is often entirely reversible; i.e., the nanocrystal can be moved back and forth by simply switching the applied current polarity. The speed of the nanocrystal within the nanotube is dependent upon the applied current magnitude. From an applications view, the mechanism is of great interest because it provides an especially convenient method of controlling the nanocrystal's position and motion with a single external electrical control parameter. Controlled movement of metal nanocrystals inside carbon nanotubes could potentially be used for nanomachine actuators [9], memory elements [3], or dispensing small quantities of metals [1] to a selected location.

The transport of metal nanocrystals within nanotubes is conventionally demonstrated for nanotubes which have a relatively smooth, uniform diameter hollow core, within which the nanocrystal can easily slide. A critical question, however, is what happens when the nanotube core contains a constriction smaller than the incoming nanocrystal cross section. The naive answer is that if the nanocrystal remains solid it will be completely blocked by the constriction, while if it is heated beyond its melting point and becomes liquid it might (assuming surface tension energies can be overcome) squeeze through. We here demonstrate how a metal nanocrystal, while remaining solid and crystalline, can in fact be made to slip through a very small constriction through which it should not geometrically fit. The squeezing mechanism is decidedly not one of severe deformation and plastic flow, but rather a form of atomic level deconstruction at the crystal's trailing edge and reconstruction at the leading edge. Indeed, this deconstruction and reconstruction of surface atoms is a continual process even without a constriction: It can be the dominant mechanism by which the electrical current transports the metal nanocrystal through any nanotube bore, smooth or not.

To demonstrate transport of iron nanocrystals through a carbon nanotube constriction experimentally, we fabricate a two-terminal nanotube device suitable for insertion into a high resolution transmission electron microscope (JEOL 2010) with nanodiffraction and dark field analysis capability. Multiwall carbon nanotubes containing iron nanoparticles are grown by pyrolysis of ferrocene in an inert gas atmosphere at 1000 °C. Such nanotubes often have naturally occurring constrictions within their interior (e.g., where the number of tube walls abruptly changes). The nanotubes that contain iron nanocrystals are then deposited onto thin silicon nitride membranes, and electrical contacts are formed using electron beam lithography. The resulting two-terminal nanotube device is driven with a dc electrical current during TEM imaging, which allows observation and control of nanoparticle motion in real time. The nitride membrane platform allows the same device to be measured multiple times and affords mechanical stability during TEM imaging.

We observe that injecting the electrical current axially to the nanotube causes the iron nanoparticle to move in the direction of the electron flow. The velocity varies with the current nonlinearly, and the motion of the nanoparticle is reversible, consistent with previous observations [3,4]. We also observe the movement of iron nanoparticles into and through narrow constrictions within the nanotube, as demonstrated in Fig. 1. Figure 1(a) shows a TEM image of a multiwall carbon nanotube with an approximately 45 nm

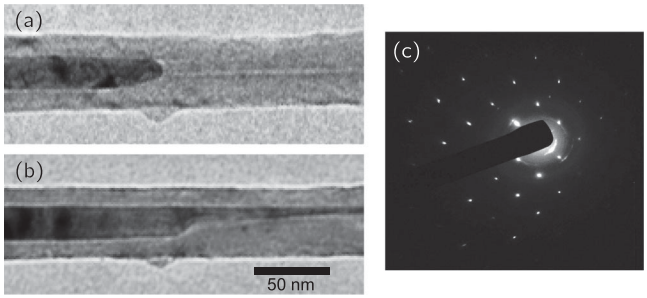

FIG. 1. Microscopy and diffraction of a nanotube system. (a) Shown is a transmission electron micrograph of an iron nanocrystal (darker contrast that spans the left half of the image) inside a multiwalled carbon nanotube. (b) Shown is the same section of nanotube after a current has been applied, causing the iron nanoparticle to squeeze into the adjacent constriction. The iron nanocrystal (darker contrast) now spans the full image width. (c) Shown is a diffraction pattern for a different iron nanoparticle while moving through a nanotube constriction, confirming its crystallinity.

outer diameter. The nanotube core on the left side of the image is approximately 20 nm in diameter, and it is filled with iron (dark contrast). Midway along the axis of the nanotube, there is clear constriction, and the core reduces to about 5 nm. In Fig. 1(a), the iron nanoparticle borders this constriction, and the reduced inner diameter core is empty beyond. Figure 1(b) shows the same nanotube region several seconds later; the iron nanoparticle has advanced to the right and has infiltrated the narrow core region beyond the constriction (also now dark contrast). Numerous similar iron infiltrations into and past constrictions are observed for different samples. In general, the current-driven iron nanoparticle squeezes into the constriction and continues to advance. If there is sufficient space beyond the constriction, the entire iron nanoparticle moves through the constrictions and emerges out the other side, and then continues to transport along the core of the nanotube. In order to determine the state (solid or liquid) of the iron during transport, including while infiltrating the constriction, nanodiffraction experiments are performed *in situ*. Figure 1(c) shows an example (for a different iron nanoparticle) within a nanotube constriction; the diffraction pattern is consistent with solid iron in the bcc phase, even for the portion squeezing through the constriction. Additionally, real-time dark field imaging is performed using one of the bcc iron diffraction spots, which confirms the crystallinity of the iron during transport and squeezing though the constriction. The iron nanoparticle is solid, crystalline, and lattice undeformed as it squeezes through the constriction.

Although the experiment is performed at room temperature, there is a possibility that the nanotube with the iron nanoparticle is heated due to Joule heating from the electrical current. Using the parameters of the experiment, a detailed analysis [10] reveals that the iron nanocrystal of Figs. 1(a) and 1(b) is at most at temperature $T \approx 440$ K while it squeezes though the constriction. This temperature is well below the melting point of iron of this size ($T_{\mathrm{melt}} \approx 1800$ K), consistent with the nanodiffraction and dark field imaging results, always indicating a solid crystalline state.

We now seek to understand why an iron nanocrystal can move through a constriction in a carbon nanotube with a smaller cross-sectional area than the nanocrystal itself. We first examine the microscopic origin of iron atom movement inside the carbon nanotube with a smooth bore and then adapt the model to constrictions. We perform a series of first principles density functional theory [11,12] calculations, followed by a kinetic Monte Carlo simulation [13,14].

We use density functional theory calculations to compute the energy barriers for iron atom diffusion in various environments. We examine bulk diffusion, diffusion on different iron surface orientations, and diffusion at the iron-carbon interface. We also use density functional theory calculations to obtain estimates of the iron-iron and the iron-carbon binding energies. Once we obtain these parameters, we extract trends of diffusion energy barriers and binding energies, and construct an algorithm to assign a diffusion barrier height to arbitrary diffusion processes in iron. Next, using this algorithm for the assignment of diffusion barrier heights, we perform kinetic Monte Carlo simulations of an iron nanocrystal inside a carbon nanotube. The kinetic Monte Carlo method, unlike the static density functional theory method, allows us to perform a time-evolution study of the movement of the iron nanocrystal.

In the simulation, we assume that the electromigration force F experienced by individual iron atoms is linearly proportional to the current density j; $F = jK$, and we obtain a parameter K by fitting the results of our simulation to the experiment. (The linear dependence of force F on current density j is consistent with an electron wind force mechanism [15,16].) Furthermore, we assume that the electromigration force F affects the iron atom movement by increasing or decreasing the iron diffusion barrier height according to the work done by F along the atom diffusion path. The depth of the contact region in which iron atoms are experiencing the electromigration force F does not affect the resulting speed of the nanocrystal but only its instability toward breaking (a deeper contact region produces an earlier onset of instability). Details of this combined density functional theory and kinetic Monte Carlo calculation will be presented elsewhere [17]. The microscopic results of the kinetic Monte Carlo simulations are shown in Figs. 2 and 3. Figure 2 schematically shows the nature of the movements of the iron atoms. We find that, for most of the time, any given iron atom is stationary, as shown in Fig. 3. Once the stationary bulk iron atoms are exposed to the surfaces, they quickly move from the left end of the nanocrystal (as in Fig. 2), along the contact

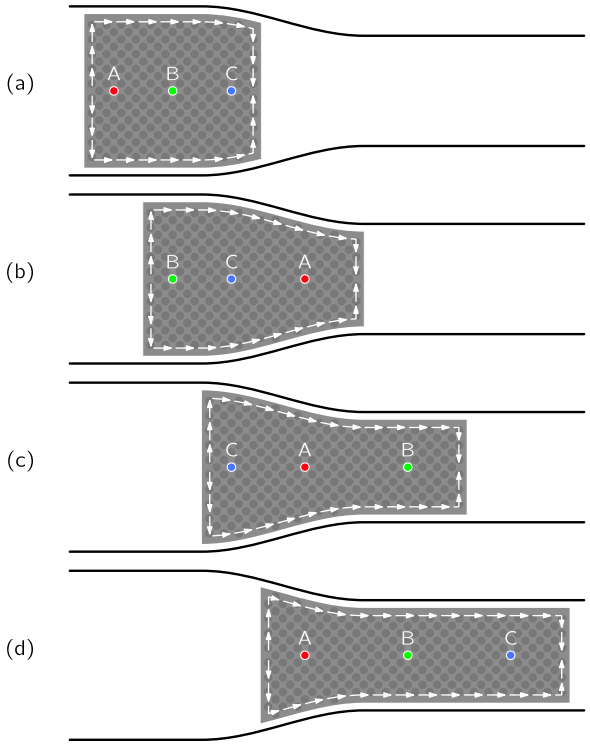

FIG. 2 (color online). Sketch of iron nanocrystal movement. (a)–(d) Schematically shown are four consecutive time snapshots of a solid iron nanocrystal (gray regions) moving through a constriction in a carbon nanotube (outer black curves). Atoms in the bulk of the nanocrystal remain stationary as long as they are in the bulk. Once iron atoms from the bulk are exposed to the end surface on the left side of the crystal, they quickly move along the nanocrystal surface and contact region with the carbon nanotube to the right end of the crystal (white arrows). For illustration purposes, instantaneous positions of three selected iron atoms are indicated with red, green, and blue circles and with capital letters A, B, and C. In each of the four panels, the three selected iron atoms are in the bulk of the nanocrystal, illustrating the fact that, compared to time spent in the bulk, surface movement is nearly instantaneous. Movement of iron atoms in the contact region with the carbon nanotube originates from the electromigration force. Additionally, this force creates a concentration gradient that drives the diffusion from the left (right) end of the crystal toward (away from) the contact region (see also Fig. 3).

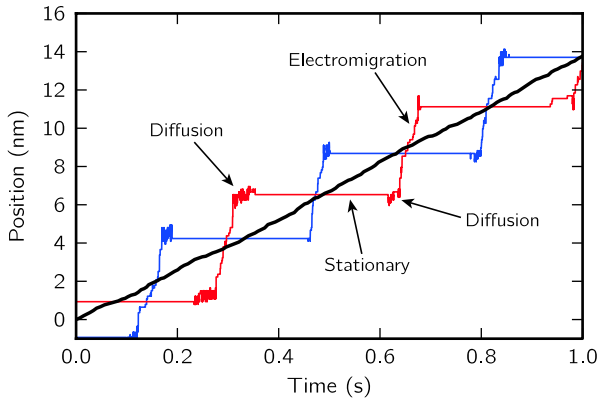

FIG. 3 (color online). Movement of individual iron atoms. The thin (red and blue) lines show the simulated positions along the carbon nanotube axis of two randomly selected iron atoms as a function of time. The thick black line shows the average position (center of mass) of all iron atoms in the simulation. The average position of the iron atoms is continuously increasing. On the other hand, individual iron atoms remain stationary most of the time. It is only when they are exposed to the surface that they move quickly across the entire length of the crystal by a combination of diffusion and electromigration forces (see also Fig. 2). This kinetic Monte Carlo simulation is performed at a temperature of 600 K, the electromigration force on the iron atoms is 0.33 eV/nm, and the iron nanocrystal radius is $r_{\mathrm{cyl}} = 1.05$ nm, while its length is $l = 4.31$ nm.

region with the carbon nanotube, toward the right end of the crystal. Since iron atoms are depleted from the left surface, they expose a new layer of bulk atoms to the surface, which then start to move in the same way. Analogously, when these atoms arrive to the right surface, they soon become buried under layers of new incoming iron atoms, and thus they once again become part of the bulk and become stationary. The nanocrystal is deconstructed at the left and reconstructed at the right, and the surface atoms overtake their bulk counterparts. Hence, the nanocrystal moves, even though virtually all of the atoms comprising the nanocrystal (i.e., all but the surface atoms) remain stationary in the laboratory frame. A somewhat related mechanism, but one involving the heating of an iron nanocrystal and its chemical interaction with the carbon nanotube, was recently proposed in Ref. [4].

The origin of the surface movement of iron atoms is twofold. In the contact region with the carbon nanotube, iron atoms move due to the influence of the electromigration force from the applied current. On the exposed iron surfaces on both the left and right sides of the nanocrystal, movement is driven by the diffusion forces. Diffusion forces away from the left side and toward the right side of the nanocrystal are originating in the iron atom concentration gradient created by the electromigration force in the contact region with the carbon nanotube. The pattern of iron atom movement presented above explains why the iron nanocrystal can move through a constriction while remaining solid. If the iron nanocrystal were moving as a whole, it would have to deform in order to go through a constriction. On the other hand, the mechanism we consider does not require deformation of the crystal. Instead, once the iron nanocrystal reaches a constriction, new atoms are transported toward the region within the smaller cross-sectional area, and they assemble there to form new layers of iron atoms that adjust their cross-sectional area to match the constriction.

Our theoretical modeling allows us to analyze the dependence of the iron nanocrystal center of mass speed on various external parameters. First, we find that the iron

nanocrystal center of mass speed does not depend on the nanocrystal length. This observation is easily explained by the fact that the electromigration force driven motion of iron atoms in the contact region is much more effective than the diffusion on the two ends of the nanocrystal. Second, in our simulations we find an exponential thermally activated dependence of the center of mass speed v on the electromigration force per iron atom F and the simulation temperature T,

$$v = \tilde{v} \exp\left(-\frac{\tilde{B}}{kT}\right) \sinh\left(\frac{\frac{1}{2}\tilde{L}F}{kT}\right). \quad (1)$$

Fitting this equation to the results of our simulation, we obtain the following values of the $\tilde{v}$, $\tilde{B}$, and $\tilde{L}$ parameters:

$$\tilde{v} = 3.3 \text{ m/s}, \qquad \tilde{B} = 1.2 \text{ eV}, \qquad \tilde{L} = 1.4 \text{ nm}. \quad (2)$$

The functional form given in Eq. (1) is the same as that of a single particle coupled to a thermal bath at temperature T moving in a periodic tilted washboard potential [18] [shown in Figs. 4(a) and 4(b)] with period $\tilde{L}$, barrier height $\tilde{B}$, and under the influence of a constant force F. Finally, we find a complex dependence of the center of mass speed on the cross-sectional area of the iron nanocrystal (with an overall trend of decreasing center of mass speed with increasing cross-sectional area). The origin of this complex dependence comes from the fact that, depending on the radius of the iron nanocrystal, one obtains different iron surface morphologies with varying diffusion pathways in the contact region with the carbon nanotube. Nevertheless, we find that varying the cross-sectional area of the iron nanocrystal mostly influences the value of the parameter $\tilde{v}$ in Eq. (1), while $\tilde{B}$ and $\tilde{L}$ are essentially unchanged. Since the parameter $\tilde{v}$ appears only as a prefactor in Eq. (1), when fitting our model calculation to experiment [3,4], the precise value of parameter $\tilde{v}$ will be almost irrelevant compared to $\tilde{B}$ and $\tilde{L}$. Thus, even though the motion of individual iron atoms in a carbon nanotube is quite complex, the effective speed of the entire iron nanocrystal can be simply modeled as that of a single particle in a tilted washboard potential.

Extrapolating our model calculation to the experimental regime of parameters, we find good agreement with experiment [3] using a temperature of 350 K and a constant of proportionality $K = 0.18$ eV nm/μA between the current density through the iron nanocrystal and the electromigration force [see Fig. 4(c)]. To obtain this value of parameter K (0.18 eV nm/μA), we crudely estimated the current density through the iron nanocrystal based on the resistivity of *bulk* iron and graphite, the nanotube geometry, and assuming a constant current density profile perpendicular to the nanocrystal axis. There is thus a large uncertainty in the assumed current density and hence K. We are unaware of any previous theoretical or experimental estimates of parameter K in iron. Moreover, theoretical estimates [16,19] of parameter K for studied elemental metals vary widely across the periodic table in magnitude and even in sign. Furthermore, the value of parameter K is very sensitive [16] to the atomic structure and differs for the self-electromigration and electromigration of an impurity. Interestingly enough, the largest value of parameter K obtained in Ref. [16] is that of iron impurity electromigrating in aluminum (0.01 eV nm/μA), which is within an order of magnitude to the value we obtained.

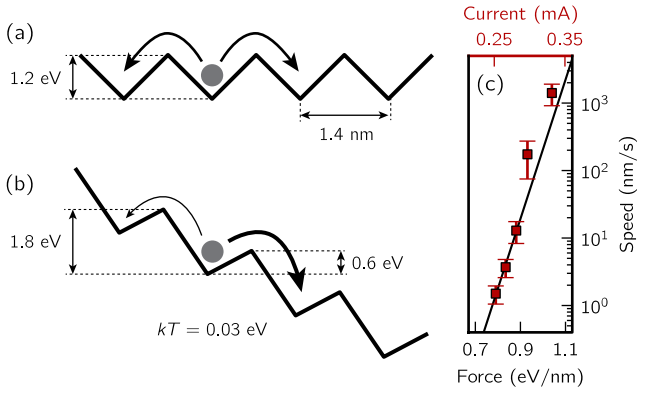

FIG. 4 (color online). The complex motion of an iron nanocrystal shown in Figs. 2 and 3 can be simply modeled as the movement of a single particle in an effective periodic external potential with the barrier height $\tilde{B}$ of 1.2 eV and the period $\tilde{L}$ of 1.4 nm (assuming that the force experienced by a single iron atom is applied to this effective particle). This is true regardless of the iron nanocrystal length, cross-sectional area, temperature, and magnitude of the electromigration force. (a) When the electromigration force is not present, the particle behaves as if it is in an untilted washboard potential with equal energy barriers in the left and right directions. (b) When the electromigration force F is present, the washboard potential is tilted with slope F and the barrier heights become asymmetric, which prefers the motion of the particle along the direction of F. For a typical experimental situation [3], asymmetry in the effective barrier heights is about half of the untilted barrier height ($\pm$ 0.6 eV), while the temperature is much smaller than both, only 0.03 eV. This regime of barrier heights explains the very strong observed exponential dependence of the iron nanocrystal speed on the electromigration force magnitude [3,4]. (c) Shown is the iron nanocrystal speed on a logarithmic scale as a function of the electromigration force magnitude F (black line) and the net current through the carbon nanotube (red squares). The black line is a fit to Eq. (1), with $T = 350$ K, while the red squares are measurements from Ref. [3].

Comparing values of $\tilde{B}$, $\frac{1}{2}\tilde{L}F$, and kT, we find that, in a typical experimental situation [3], the energy barrier $\tilde{B}$ is the largest, 1.2 eV. The tilt of the washboard potential due to electromigration force ($\frac{1}{2}\tilde{L}F$) equals $\pm$0.6 eV and is comparable to the barrier $\tilde{B}$ itself, while the temperature energy scale kT is an order of magnitude smaller than both, 0.03 eV. This order of energy scales [also shown in Figs. 4(a) and 4(b)] together with Eq. (1) explains the origin of the experimentally found extremely sharp onset of iron nanocrystal movement as a function of applied electric current [3,4] [see also Fig. 4(c)].

External electric control of movement of an iron nanocrystal is interesting from both fundamental science and applications viewpoints. The ability of an iron nanocrystal to remain crystalline while moving through tubes and constrictions could allow for more stable operation of nanoelectromechanical devices and opens up a possibility to explore more complex geometries than the limited geometries discussed here. Additionally, the intricate mechanism of iron nanocrystal movement could be used to refine metallic nanoparticles. For example, constant regrowth of the iron nanoparticle during its movement in the carbon nanotube could be used to remove contaminants and domain boundaries or, potentially, to introduce them with very fine spatial control. Additionally, it may be interesting to explore systems with diffusion of multiple metallic species both theoretically and experimentally.

We thank Gavi Begtrup for assistance with sample preparation and microscopy and David Strubbe for discussion. This work was supported by the Director, Office of Energy Research, Office of Basic Energy Sciences, Materials Sciences and Engineering Division, of the U.S. Department of Energy under Contract No. DE-AC02-05CH11231.

*sinisa@civet.berkeley.edu

[1] K. Svensson, H. Olin, and E. Olsson, Phys. Rev. Lett. **93**, 145901 (2004).
[2] G. E. Begtrup, W. Gannett, J. C. Meyer, T. D. Yuzvinsky, E. Ertekin, J. C. Grossman, and A. Zettl, Phys. Rev. B **79**, 205409 (2009).
[3] G. E. Begtrup, W. Gannett, T. D. Yuzvinsky, V. H. Crespi, and A. Zettl, Nano Lett. **9**, 1835 (2009).
[4] M. Loffler, U. Weissker, T. Muhl, T. Gemming, J. Eckert, and B. Buchner, Adv. Mater. **23**, 541 (2011).
[5] D. Golberg, P. Costa, M. Mitome, S. Hampel, D. Haase, C. Mueller, A. Leonhardt, and Y. Bando, Adv. Mater. **19**, 1937 (2007).
[6] C. Jin, K. Suenaga, and S. Iijima, Nat. Nanotechnol. **3**, 17 (2007).
[7] B. C. Regan, S. Aloni, R. O. Ritchie, U. Dahmen, and A. Zettl, Nature (London) **428**, 924 (2004).
[8] M. Sun and Y. Gao, Nanotechnology **23**, 065704 (2012).
[9] B. C. Regan, S. Aloni, K. Jensen, R. O. Ritchie, and A. Zettl, Nano Lett. **5**, 1730 (2005).
[10] G. E. Begtrup, K. G. Ray, B. M. Kessler, T. D. Yuzvinsky, H. Garcia, and A. Zettl, Phys. Rev. Lett. **99**, 155901 (2007).
[11] J. M. Soler, E. Artacho, J. D. Gale, A. Garcia, J. Junquera, P. Ordejon, and D. Sanchez-Portal, J. Phys. Condens. Matter **14**, 2745 (2002).
[12] K. Lee, E. D. Murray, L. Kong, B. I. Lundqvist, and D. C. Langreth, Phys. Rev. B **82**, 081101 (2010).
[13] A. Bortz, M. Kalos, and J. Lebowitz, J. Comput. Phys. **17**, 10 (1975).
[14] J. L. Blue, I. Beichl, and F. Sullivan, Phys. Rev. E **51**, R867 (1995).
[15] R. S. Sorbello, in *Theory of Electromigration*, Solid State Physics Vol. 51, edited by H. Ehrenreich and F. Spaepen (Academic, New York, 1997), p. 159.
[16] J. P. Dekker and A. Lodder, J. Appl. Phys. **84**, 1958 (1998).
[17] S. Coh, S. G. Louie, and M. L. Cohen, arXiv:1304.6438.
[18] H. Risken, *The Fokker-Planck Equation: Methods of Solution and Applications* (Springer, Berlin, 1996), Vol. 18.
[19] R. Sorbello, J. Phys. Chem. Solids **34**, 937 (1973).